

Equatorward shift of the South Asian high in response to anthropogenic forcing

**Xia Qu, Gang Huang, Kaiming Hu,
Shang-Ping Xie, Yan Du, Xiao-Tong
Zheng & Lin Liu**

Theoretical and Applied Climatology

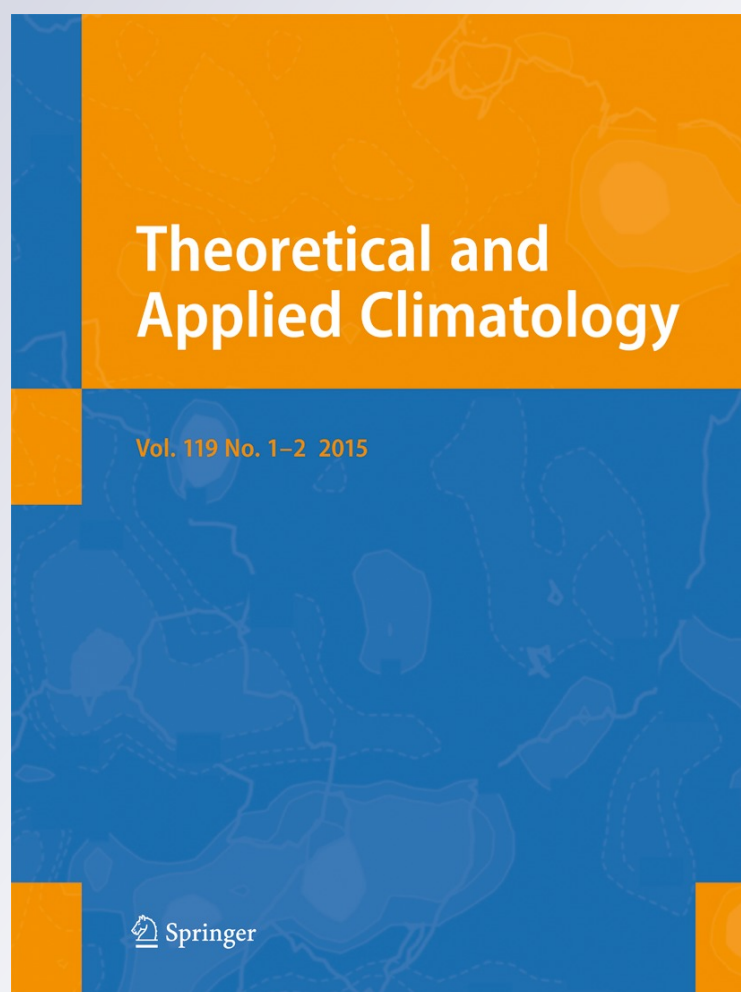
ISSN 0177-798X

Volume 119

Combined 1-2

Theor Appl Climatol (2015) 119:113-122

DOI 10.1007/s00704-014-1095-1



Your article is protected by copyright and all rights are held exclusively by Springer-Verlag Wien. This e-offprint is for personal use only and shall not be self-archived in electronic repositories. If you wish to self-archive your article, please use the accepted manuscript version for posting on your own website. You may further deposit the accepted manuscript version in any repository, provided it is only made publicly available 12 months after official publication or later and provided acknowledgement is given to the original source of publication and a link is inserted to the published article on Springer's website. The link must be accompanied by the following text: "The final publication is available at link.springer.com".

Equatorward shift of the South Asian high in response to anthropogenic forcing

Xia Qu · Gang Huang · Kaiming Hu · Shang-Ping Xie · Yan Du · Xiao-Tong Zheng · Lin Liu

Received: 7 February 2013 / Accepted: 20 January 2014 / Published online: 13 February 2014
© Springer-Verlag Wien 2014

Abstract The South Asian high (SAH) is a huge anticyclone in the upper troposphere. It influences the climate and the distribution of trace constituents and pollutants. The present study documents the change in the SAH and precipitation under global

warming, as well as the possible link between the changes, based on 17 Coupled Model Intercomparison Project Phase 5 (CMIP5) model simulations. The CMIP5 historical simulation reproduces reasonably the tropospheric circulation (including the SAH), precipitation, and moisture. Under global warming, more than 75 % of the CMIP5 models project a southward shift of the SAH. The southward shift is more significant in the models with stronger anticyclonic circulation in the south part of the climatological SAH. The precipitation response displays a contrasting feature: negative over the southeastern equatorial Indian Ocean (IO) and positive over the tropical northern IO, the Bay of Bengal, and the equatorial western Pacific. The results of a linear baroclinic model (LBM) show that the regional rainfall changes over the Bay of Bengal and the equatorial western Pacific have a main contribution to the southward shift of the SAH. In addition, the precipitation and the surface wind responses over the Indo-Pacific region are well coupled. On one hand, the surface wind anomaly affects the rainfall response through altering the SST and moisture. On the other hand, the condensational heating released by regional rainfall changes sustains the surface wind response.

X. Qu · K. Hu

Center for Monsoon System Research, Institute of Atmospheric Physics, Chinese Academy of Sciences, Beijing 100029, China

X. Qu

Plateau Atmosphere and Environment Key Laboratory of Sichuan Province, Chengdu 610225, China

G. Huang (✉)

Key Laboratory of Regional Climate-Environment Research for Temperate East Asia, Institute of Atmospheric Physics, Chinese Academy of Sciences, Beijing 100029, China
e-mail: hg@mail.iap.ac.cn

S.-P. Xie · X.-T. Zheng

Physical Oceanography Laboratory and Ocean-Atmosphere Interaction and Climate Laboratory, Ocean University of China, Qingdao 266100, China

Y. Du

Key Laboratory of Tropical Marine Environmental Dynamics, South China Sea Institute of Oceanology, Chinese Academy of Sciences, Guangzhou 510301, China

L. Liu

The First Institute of Oceanography, State Oceanic Administration, Qingdao 266061, China

G. Huang

Collaborative Innovation Center on Forecast and Evaluation of Meteorological Disasters, Nanjing University of Information Science & Technology, Nanjing 210044, China

S.-P. Xie

International Pacific Research Center and Department of Meteorology, University of Hawaii at Manoa, Honolulu, Hawaii

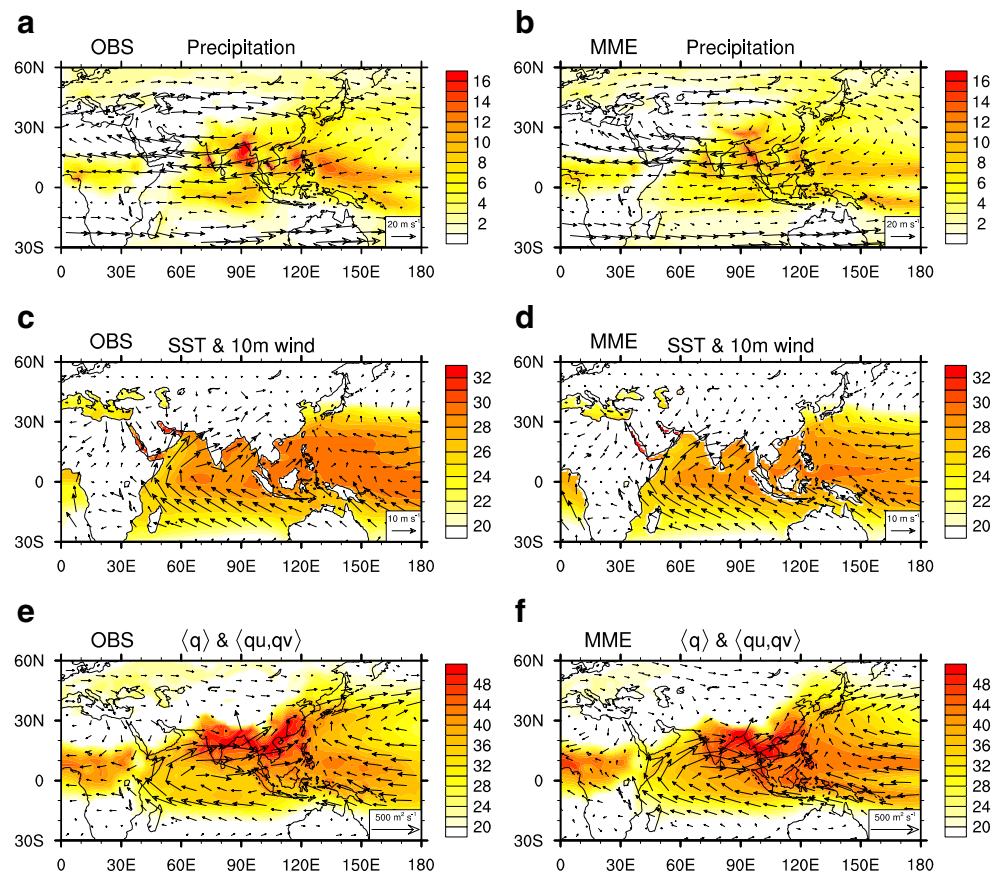
S.-P. Xie

Scripps Institution of Oceanography, University of California, La Jolla, San Diego, CA, USA

1 Introduction

In boreal summer, a huge anticyclone exists in the upper troposphere and the lower stratosphere over the Tibetan Plateau and the surrounding area (Fig. 1a). This high pressure system, called the South Asian high (SAH) or the South Asian anticyclone, forms due to the heating of the Tibetan Plateau and the South Asian monsoon precipitation (Flohn 1960; Hoskins and Rodwell 1995; Duan and Wu 2005; Boos and Kuang 2010). It is the strongest and steadiest system in the upper troposphere (Mason and Anderson 1963; Li et al. 2005). The SAH determines the global pattern of several trace constituents and pollutants in the upper troposphere and the lower stratosphere. For instance, the tropical and subtropical jets, residing on the south

Fig. 1 The climatology of **a, b** precipitation (color shaded, unit: millimeters per day) and 100 hPa wind (vector); **c, d** SST (color shaded, unit: degree Celsius) and 10 m wind (vector); and **e, f** integration of specific humidity (color shaded, unit: kilogram meter per kilogram) and moisture transport (vector) from surface to 100 hPa in 1979–2004. **a, c, e** Results of NCEP-NCAR reanalysis or HadISST; **b, d, f** are the results of the CMIP5 MME. The reference vectors are shown in the *bottom-right corners* of each figure. $\langle \rangle$ in the titles of **e** and **f** means a mass integration from surface to 100 hPa



and north flanks of the SAH, form a barrier for meridional transports of such constituents as water vapor and ozone (Dethof et al. 1999; Randel and Park 2006). Consequently, carbon monoxide, which is transported from the lower troposphere to the upper troposphere, is trapped in the center of SAH, leading to the maximum concentration there (Park et al. 2004; Li et al. 2005). The subtropical westerly jet on the north flank of the SAH is an important circulation system in the formation and maintenance of the important climatic phenomenon of East Asia—the Meiyu-Baiu rainband (Sampe and Xie 2010) that brings the major rainy season to the densely populated region.

The SAH modulates the variation of the western Pacific subtropical high (Tao and Zhu 1964; Jiang et al. 2011) which is an important system in the East Asian summer monsoon variability (Tao and Chen 1987; Huang and Wu 1989; Huang and Sun 1992; Wu and Chen 1998) and the occurrence of severe floods and droughts in East Asia (Huang et al. 1999). In year-to-year variations, an intensified SAH leads to a strengthened western Pacific subtropical high (Zhao et al. 2009). Consequently, rainfall over the western North Pacific decreases and precipitation over subtropical East Asia increases (Zhang et al. 2005; Zhao et al. 2007). In addition, studies suggested that interannual SAH variability is associated with the South Asia monsoon, the mid-Pacific trough, and the Mexico high (Zhang et al. 2005; Zhao et al. 2007).

Greenhouse gases have been steadily increasing, causing a rise in global surface temperature. The warming, however, is not uniform due to the different properties of the Earth's surface, such as the small heat content of land and evaporation of the ocean. This may result in an inhomogeneous response in the atmosphere. In turn, this may provide feedback on the temperature change. Rather complicated are the influences of the increasing greenhouse gases on climate, including the SAH. This study addresses two specific questions about the SAH: how does the SAH respond to the anthropogenic forcing? What processes cause the response? Using the Coupled Model Intercomparison Project phase 5 (CMIP5; Meehl et al. 2009), the questions are addressed.

The paper is organized as follows: Section 2 introduces the data and methods used in the study. Section 3 evaluates the skill of the CMIP5 models. Sections 4 and 5 present the response of the SAH and precipitation, respectively. Section 6 investigates the linkage between the upper troposphere circulation and the precipitation. Section 7 provides the conclusion and discussion.

2 Data and methods

This investigation is based on CMIP5 outputs. The information for the CMIP5 models is listed in Table 1. The

Table 1 Climate models and the spatial correlation coefficients. The last row gives the information of MME

Model ID	Country	Spatial correlation coefficients based on vorticity _[0–60°N, 0–180°E] at 100 hPa
CanESM2	Canada	0.89
CNRM-CM5	France	0.88
CSIRO-Mk3-6-0	Australia	0.90
FGOALS-s2	China	0.81
GFDL-CM3	USA	0.88
GFDL-ESM2G	USA	0.91
GISS-E2-R	USA	0.79
HadGEM2-CC	UK	0.82
HadGEM2-ES	UK	0.83
inmcm4	Russia	0.71
IPSL-CM5A-LR	France	0.83
MIROC-ESM	Japan	0.80
MIROC-ESM-CHEM	Japan	0.80
MIROC5	Japan	0.90
MPI-ESM-LR	Germany	0.92
MRI-CGCM3	Japan	0.84
NorESM1-M	Norway	0.87
MME	\	0.85

experiments used in this study are historical and RCP45 scenario simulations. The historical experiments were conducted based on observed anthropogenic and natural forcing from the mid-nineteenth century to about 2006. The RCP45 experiments were conducted from 2006 to at least 2099 driven by prescribed forcing (Thomson et al. 2011). For detailed information, readers are referred to the following website: <http://cmip-pcmdi.llnl.gov/cmip5/>.

The latitude of the SAH ridge is defined as the averaged latitude of 0 m s^{-1} zonal wind over the domain $[10^{\circ}\text{--}60^{\circ}\text{N}, 0\text{--}180^{\circ}\text{E}]$ at 100 hPa. The center latitude of the SAH is defined as latitude of the maximum in 100 hPa geopotential height over the domain $[10^{\circ}\text{--}60^{\circ}\text{N}, 0\text{--}180^{\circ}\text{E}]$.

The difference between climatology of future (2069–2098) and present-day simulations (1975–2004) is used to represent the model responses to the anthropogenic forcing. Only the run “r1i1p1” of each model is analyzed. The multi-model ensemble (MME) approach is used to reduce natural variability and systematic biases in the models. The model outputs are interpolated onto a $1.0^{\circ}\times 1.0^{\circ}$ grid using a bilinear interpolation technique. The analysis is focused on summer (i.e., June–July–August) mean. The performance of CMIP5 models are evaluated against (1) the National Centers for Environmental Prediction–National Center for Atmosphere Research (NCEP–NCAR) atmospheric reanalysis with a horizontal resolution of $2.5^{\circ}\times 2.5^{\circ}$ (Kalnay et al. 1996); (2) the Center for Climate Prediction Merged Analysis of Precipitation (CMAP) with a

horizontal resolution of $2.5^{\circ}\times 2.5^{\circ}$ (Xie and Arkin 1997); and (3) the Hadley Center Global Sea Surface Temperature (HadISST) dataset with a horizontal resolution of $1.0^{\circ}\times 1.0^{\circ}$ (Rayner et al. 2006).

A linear baroclinic model (LBM) is employed in the study. The LBM is built up by atmospheric primitive equations and allows one to examine a linear dynamics in the atmosphere, such as the steady linear response to a prescribed forcing, eigenanalysis, and so on. In this study, the component of steady forcing is adopted to investigate the possible contribution of prescribed precipitation change to the SAH response. The model has a horizontal resolution of T42 and 20 sigma (σ) levels in the vertical. The climatology in the LBM is the same as the summer mean of the CMIP5 MME in 1975–2004. The horizontal diffusion has an e -folding decay time of 6 h for the largest wavenumber. The Rayleigh friction and Newtonian damping has a time scale of (0.5 day^{-1}) for $\sigma \geq 0.9$ and $\sigma \leq 0.02$ and (30 day^{-1}) for $0.02 < \sigma < 0.9$. The vertical diffusion is set at $(1,000 \text{ day}^{-1})$ at all levels. Details of the model information are given in Watanabe and Kimoto (2000). The response in the LBM reaches steady state at day 15, and the 15–24-day mean results are shown as the steady forcing to prescribed heating source.

3 The present-day climate

Before analyzing the response of the SAH to greenhouse gas forcing, we examine the performance of models based on the CMIP5 MME. Panels a and b of Fig. 1 compare the climatology of the winds at 100 hPa between the NCEP–NCAR reanalysis and CMIP5 historical simulation in 1979–2004 during which all the observational data, reanalysis, and historical simulations are available. As shown in Fig. 1a, in boreal summer, a huge anticyclone exists in the upper troposphere, extending from northern Africa to subtropical northwestern Pacific and with its center over the Tibet Plateau. The CMIP5 MME captures well the anticyclone (Fig. 1b). Based on the vorticity over the domain $[0\text{--}60^{\circ}\text{N}, 0\text{--}180^{\circ}\text{E}]$ at 100 hPa during 1975–2004, the spatial correlation is computed in each CMIP5 model and MME. The results are shown in Table 1. The CMIP5 models generally show spatial correlation coefficients spanning from 0.71 to 0.92, and the spatial correlation coefficient of MME is 0.85. The results vary a little if the correlation is computed on a smaller domain, such as $[10\text{--}50^{\circ}\text{N}, 20\text{--}120^{\circ}\text{E}]$. Hence, the CMIP5 MME is capable of reproducing the SAH's horizontal structure. Besides, Duan et al. (2013) evaluated 15 CMIP5 models and found that all are capable to simulate the climatological pattern.

In addition, we compared and examined rainfall, sea surface temperature (SST), 10 m wind, integration of humidity, and moisture transport from surface to 100 hPa, which are associated with SAH response. In boreal summer, the rainfall

over the Indo-Pacific region shows four centers: the west coast of Indian, the Bay of Bengal, the South China Sea, and the northwestern Pacific (Fig. 1a). The CMIP5 MME simulates reasonably the gross feature of the rainfall. The rainfall centers are captured except that they are a little weaker (Fig. 1b). In most part of the domain [10°S–30°N, 50–180°E], the SST is greater than 27 °C, and the CMIP5 MME can reasonably reproduce the feature (Fig. 1c, d). The 10-m wind and moisture transport over the Indian Ocean (IO) displays a C-type feature: southeasterly over the southern IO and southwesterly over the northern IO (Fig. 1c, e); over the northwestern Pacific, anticyclonic moisture transport is apparent. The observed features are well captured by the CMIP5 MME (Fig. 1d, f). For the integration of humidity of the atmospheric column, the extraordinary wet condition is prominent over South Asia and East Asia coast (Fig. 1e). This is reasonably reproduced in the CMIP5 MME, too (Fig. 1f).

Overall, the CMIP5 MME simulates well the patterns of SAH and large-scale rainfall, SST, surface wind, moisture transport, as well as moisture. We proceed to use the CMIP5 MME to investigate the response of the SAH to the anthropogenic forcing.

4 The SAH response

Under global warming, the SAH shifts southward. During the last 30 years in the twenty-first century, anomalous anticyclone is evident over the south part of the SAH's climatological

position relative to historical simulation (Fig. 2a). The anticyclone extends from North Africa to South China Sea, centering over Indian Ocean. The anomalous westerly over 30–50°N may enhance the westerly in the north part of the SAH and shifts the 0-m-s⁻¹ line of zonal wind southward. The anomalous easterly over the equatorial IO sector favors the southward expansion of easterly in the south part of the SAH. It may be expected that the SAH is equatorward under global warming. Consistently, the SAH ridge and center gradually move southward from 1975 to 2100 (Fig. 2b). The responses in individual model are given in Fig. 3. For the latitude of the SAH ridge, 14 out of 17 models project an equatorward movement under the RCP45 scenario; for the center latitude, 15 out of 17 models show a southward shift in response to anthropogenic forcing. As more than 75 % of the models project the movement with the same orientation, the response could be regarded as significant.

In addition, the 100-hPa vorticity response is analyzed. The areal mean vorticity responses are computed over the domains: [10°–30°N, 20°–120°E] and [30°–50°N, 20°–120°E], as indicated by the rectangles in Fig. 2a. The two domains are respectively named S SAH and N SAH. Over S SAH, which is the south part of the SAH's climatological position, all the 17 models show anticyclonic response (Fig. 4). Over N SAH, the responses in individual models are diverse. The anticyclonic vorticity over N SAH enhances in six models, while it weakens in 11 models (Fig. 4).

The contrast between the vorticity responses over S SAH and N SAH is linked to intensity of the southward shift of the

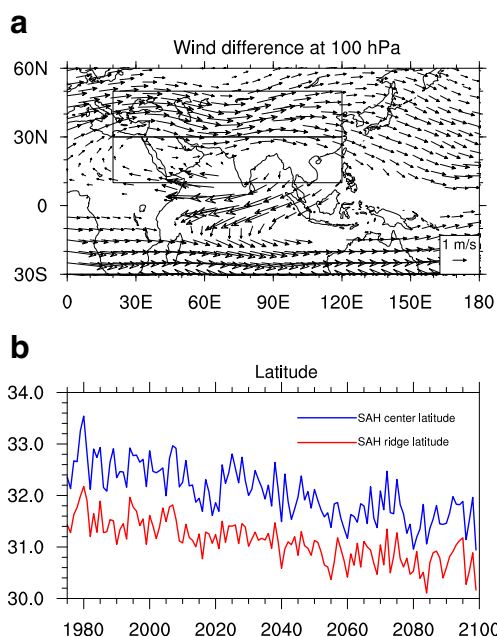


Fig. 2 a The difference of wind (vectors) between RCP45 and historical simulation at 100 hPa. Only vectors of more than 13 models projecting consistent wind direction are shown. b The CMIP5 MME time serials of SAH ridge latitude and center latitude from 1975 to 2100

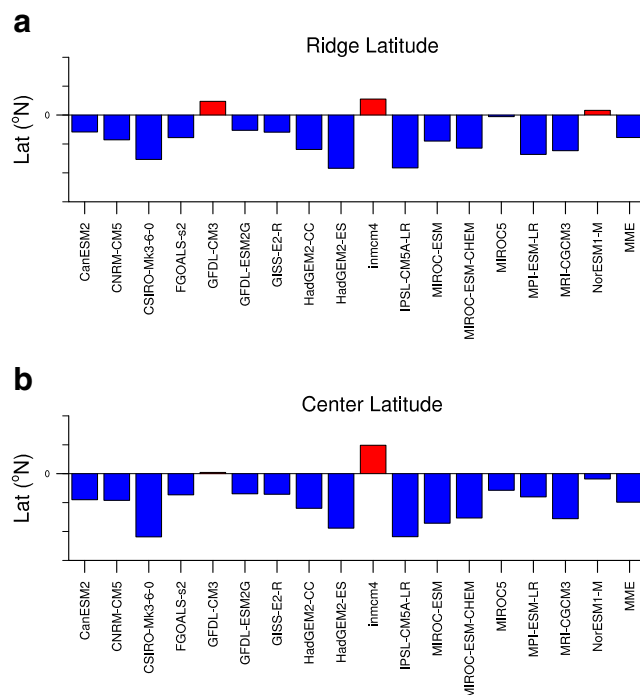


Fig. 3 The differences between RCP45 and historical simulation in each model and MME: a SAH ridge latitude (unit: degree); b SAH center latitude (unit: degree)

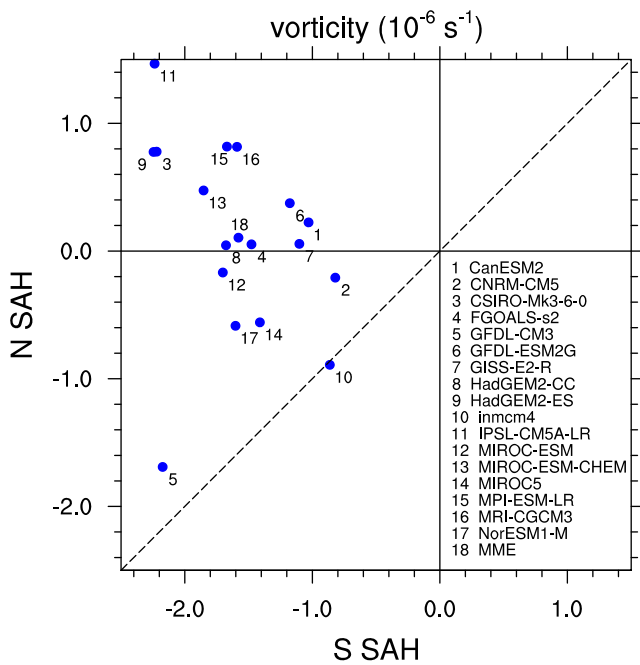


Fig. 4 The scatter plot of vorticity (unit, 10^{-6} s^{-1}) responses in RCP45 simulation. The X and Y axes denote the responses over S SAH and N SAH, respectively

SAH. In Fig. 4, the dash line means that the vorticity changes over S SAH and N SAH are equal. The dots above (below) the dash line mean that the vorticity responses over N SAH are less (greater) than that over S SAH in value. The dots, which are (not) far from the dash line, mean that the contrast of the vorticity over the two regions is large (small). The models with more significant equatorward movements of the SAH, such as CSIRO-Mk3-6-0 and IPSL-CM5A-LR, show large vorticity contrast between S SAH and N SAH. While in GFDL-CM3 and inmcm4, the two models showing little or opposite meridional shift relative to the others, the vorticity changes differ a little in the two regions. The nearly uniform change over the two domains disfavors the meridional movement of the SAH. Thus, the models with stronger anticyclonic response in S SAH than that in N SAH tend to project more significant southward movement.

5 The precipitation change

The results in Liu et al. (2001) suggested that the condensational heating is an important cause to the upper level circulation change. Thus, this section explores the associated rainfall change under the impacts of anthropogenic forcing.

The precipitation response displays a contrasting structure over the Indo-Pacific sector (Fig. 5a). Rainfall decreases over the southeastern equatorial IO and increases north of the equator, with maximums over the tropical northern IO, the Bay of Bengal, and the equatorial western Pacific. The overall precipitation pattern is dominated by the increase north of the

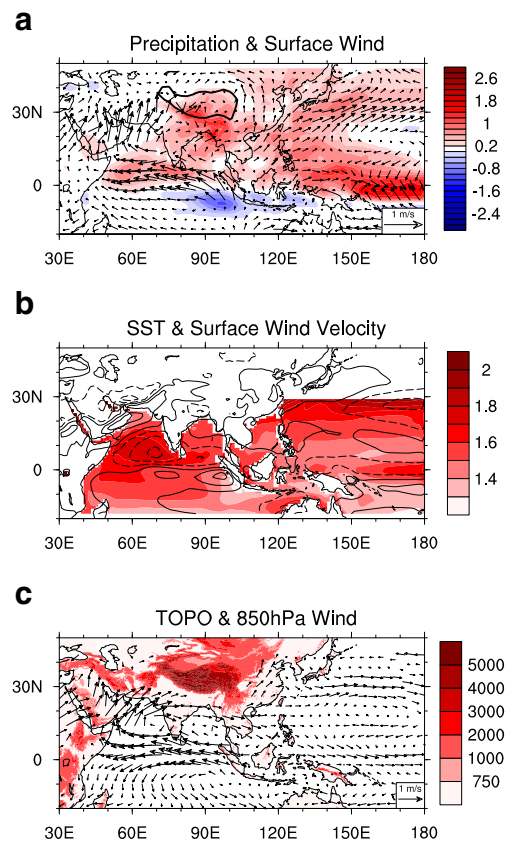


Fig. 5 The differences between RCP45 and historical simulation: **a** precipitation (color shaded, unit: millimeters per day) and surface wind vector (vectors); **b** SST (color shaded, unit: Kelvin) and surface wind velocity (black contours, unit: meters per second) and land orography (color shaded, unit: meters). The thick black contour in **a** denotes the orography is 3,000 m. In **b**, only contours for ± 0.1 , ± 0.3 , ± 0.5 , and ± 0.7 are shown and the negatives are displayed in dash contours. Besides, only the SST results south of 30°N are shown for clarity

equator. The rainfall response over the southeastern IO is not consistently projected by the models, while over the rest of the three maximum regions, more than 13 models show the same sign change (Fig. 6a). Hsu and Li (2012) investigated the rainfall change over the IO sector based on 13 CMIP5 models and showed good model consistency over both the northern IO and the southeastern IO. The present investigation shows difference over the latter region to that of Hsu and Li (2012). The selection of the models may affect the consistency.

Under global warming, one of the most robust responses is the weakening of the Walker circulation (Held and Soden 2006), with anomalous easterlies over the IO and westerlies over the equatorial Pacific (Figs. 5a, c and 6b, c). Anomalous surface easterlies reduce surface wind speed over the tropical northern IO (Fig. 5b) and the evaporation in favor of an increase in local SST. South of the equator, the acceleration of surface wind results in the enhanced evaporation and reduced SST warming (Fig. 5b). Note that the accelerated wind is not very coherent in the models. The anomalous easterlies along the equator shoal depress to the thermocline over the

equatorial eastern (western) IO, giving rise to an east–west SST gradient. The combined effect of the evaporation and thermocline shapes the SST pattern in the IO, with the largest (least) warming over the tropical northern IO (southeastern equatorial IO); besides, the reduced precipitation favors the SST increase in the southeastern IO (Fig. 5b). Over the equatorial western Pacific, the weakening of the surface wind speed favors the underlying SST warming (Fig. 5b). But the weakening is projected in less than 13 of the models. The SST

warming may be led by ocean dynamics, atmosphere warming, or exaggerated wind–SST relationship in a single model. Over the tropical IO and western Pacific oceans, the SST warming under RCP45 scenario is projected by all the models (figure not shown). The CMIP5 models are consistent in the SST change to atmosphere warming.

To explore the causes of rainfall change, we performed a diagnosis of the moisture budget. Precipitation in response to anthropogenic forcing is as follows:

$$P' = - < \bar{\omega} \partial_p q' > - < \omega' \partial_p \bar{q} > - < \omega' \partial_p q' > - < \bar{V} \cdot \nabla q' > - < V' \cdot \nabla \bar{q} > - < V' \cdot \nabla q' > + E'$$

where the overbar means climatology in 1975–2004 in historical simulation. The (') means the departure from the climatology of 1975–2004. P , ω , q , V , and E represent the precipitation, pressure velocity, specific humidity, horizontal wind, and evaporation, respectively. $< >$ means a mass integration from surface to 100 hPa.

Figure 7 shows the responses of the moisture budget terms over the four anomalous rainfall centers. For the Bay of Bengal, the rainfall change is mainly caused by enhanced moisture and it is consistently projected by the models (Fig. 7a). Under global warming, Africa and central Asia continents warm faster than the Arabian Sea due to the large heat content of water and the evaporation of the ocean. The thermal contrast leads to an enhancement of the South Asian monsoon southwesterly, bringing more moisture from the Arabian Sea to the Indian Ocean, as well as the Bay of Bengal. The southwesterly enhancement is consistently projected in more than 13 models (Fig. 6b, c). The mountains to the north of the Indian Ocean trap the water vapor south of the Himalayas, favoring the moisture accumulation. It is evident in Fig. 5a, c. Besides, the CMIP3 results in Ueda et al. (2006) project the same response. For the northern tropical IO, the anomalous precipitation also results from humidity increase (Fig. 7b). As the underlying SST warms (Fig. 5b), the saturation-specific humidity increases and the atmosphere could hold more moisture. The above causes are similar to that of global monsoon precipitation in Hsu and Li (2012). For the southeastern equatorial IO, the above rainfall change in MME arises from the anomalous descent motion (Fig. 7c), which may be caused by the less warming there (Fig. 5b). For the equatorial western Pacific, the intensified upward motion mainly contributes to the enhanced precipitation there (Fig. 7d). The ascent motion may be due to the local higher SST increase (Fig. 5b).

The condensational heating associated with the precipitation anomalies in turn sustains the anomalous circulation in the lower troposphere, which is verified by the LBM results in the next section. The interaction among the lower level wind and precipitation provides a positive feedback.

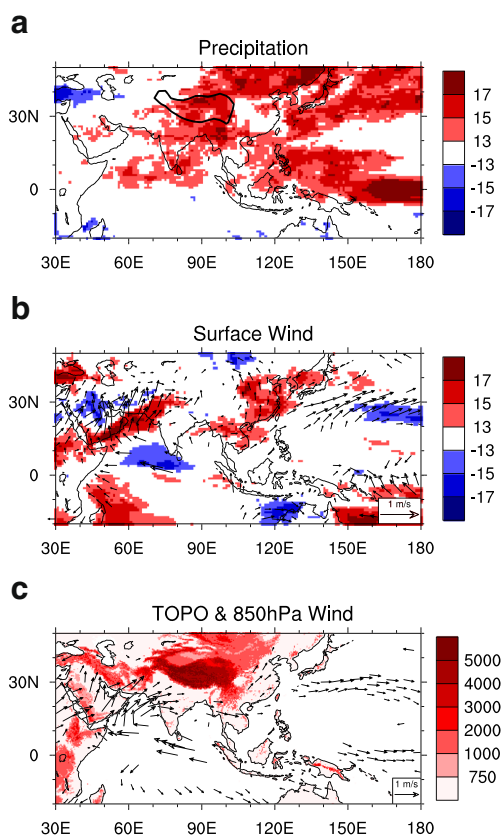
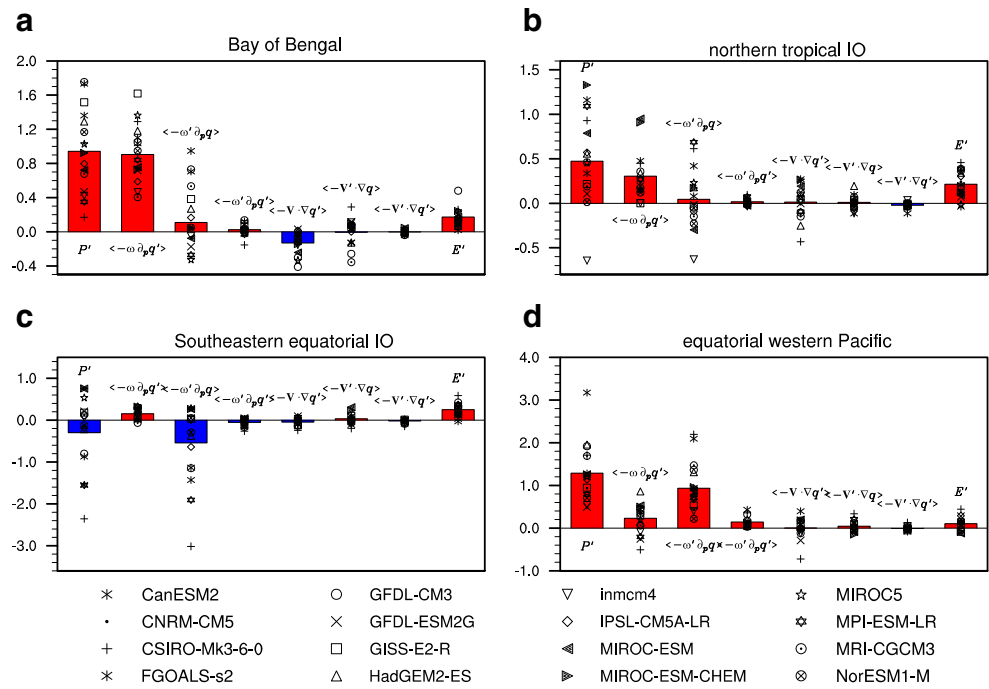


Fig. 6 The coherence (color shaded) of **a** precipitation and **b** surface wind speed under RCP45 relative to historical simulation. Red (blue) means the number of models showing the same sign response as the MME and the MME shows positive (negative) response. Vectors in **b** show the surface wind response. **c** 850 hPa wind vectors (vector) and land orography (color shaded, unit: meters). In **b** and **c**, only vectors of more than 13 models showing the same sign response are shown

6 The influences of precipitation

To investigate the effects of precipitation on circulation, the LBM is employed. The spatial distributions and intensities of

Fig. 7 The responses of the moisture budget terms in the CMIP5 MME (box charts) over **a** the Bay of Bengal [20–30°N, 80–100°E], **b** the northern tropical IO [0–10°N, 50–90°E], **c** the southeastern equatorial IO [15°S–0, 80–110°E], and **d** the equatorial western Pacific [5°S–5°N, 150–180°E]. Individual models results are shown in *dots*. The unit is millimeters per day. The results of HadGEM-CC are excluded for the lack of ω data



the prescribed forcing are designed to approximately match with those in Fig. 5a. The horizontal distribution of heating is elliptical. The maximum (minimum) heat source (sink) is set

at $\sigma=0.45$ and the patterns are shown in Fig. 8. The intensities of their centers in Fig. 7b–e are 1.0, 0.4, –0.5, and 1.2 K day^{–1}, respectively. They are approximately equivalent to rainfall

Fig. 8 The wind response at $\sigma=0.12$ in LBM to diabatic heating over: **a** all forcings combining those in **b–d**, **b** the Bay of Bengal, **c** the tropical northern IO, **d** the southeastern equatorial IO, and **e** the equatorial western Pacific. The contours show the distribution of the corresponding heat source/sink (unit: Kelvin per day) at $\sigma=0.45$. Only contours for $\pm 0.1, \pm 0.3, \pm 0.5, \pm 0.7, \pm 0.9, \pm 1.1, \text{ and } \pm 1.3$ are displayed and the negatives are shown in dash contours

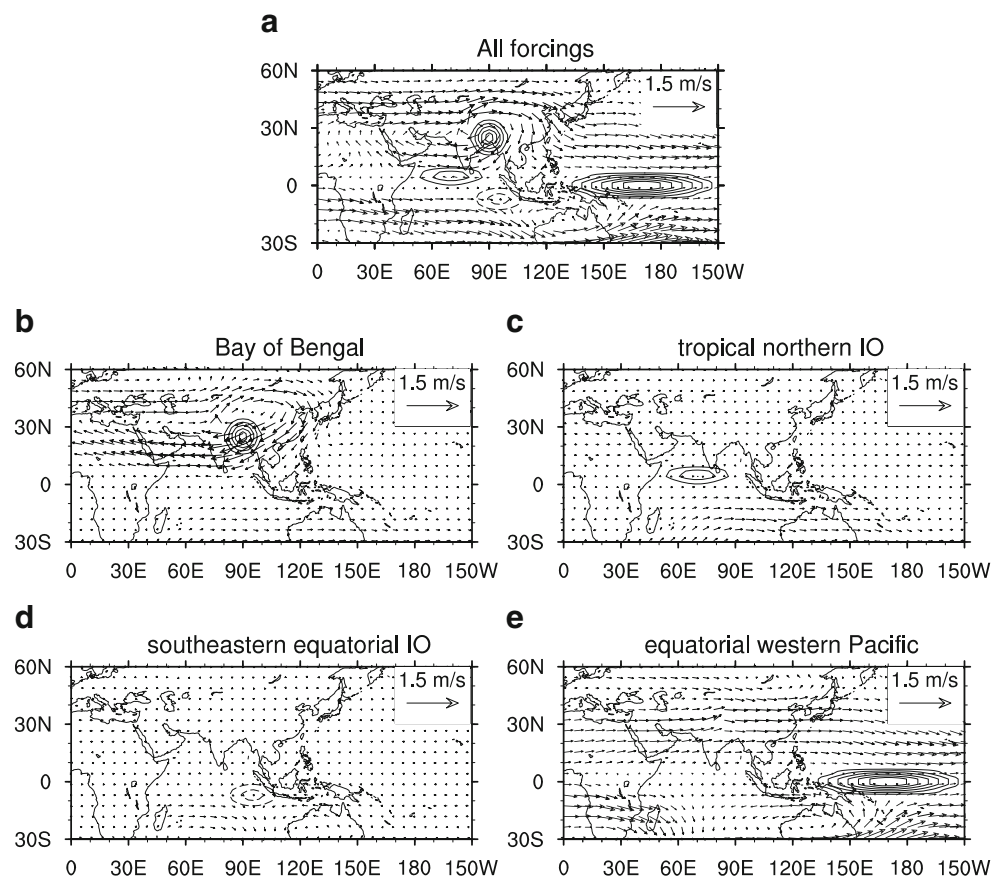
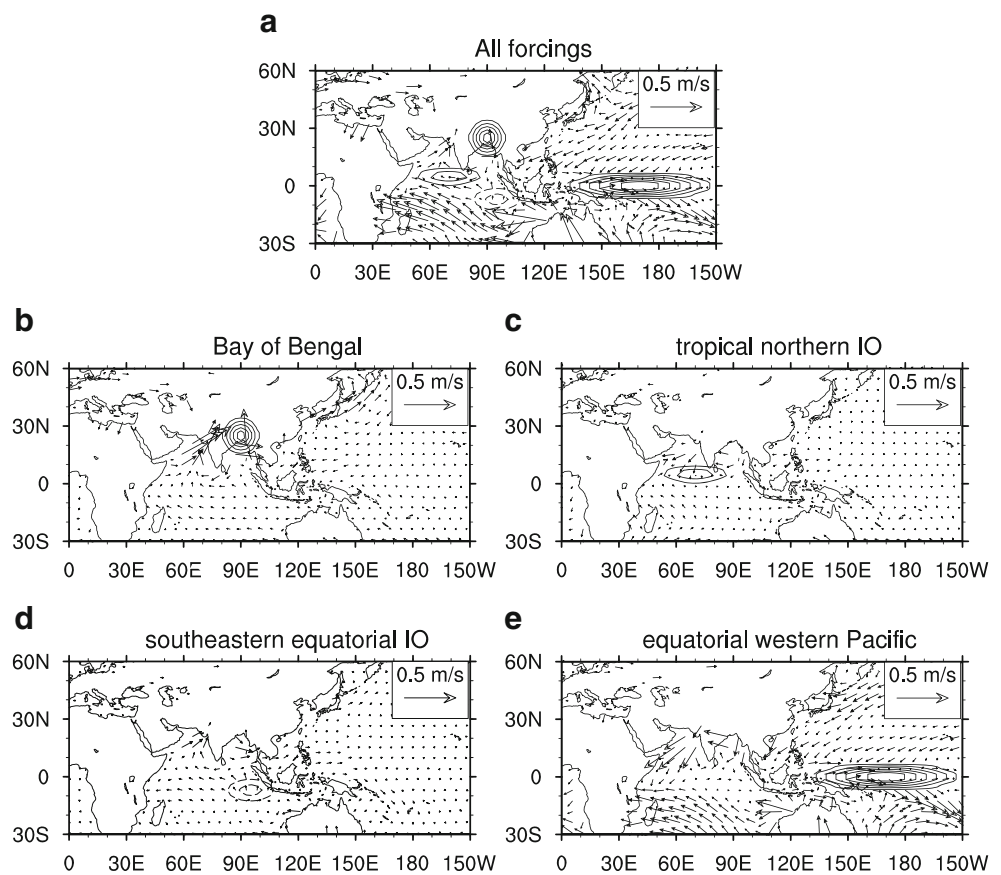


Fig. 9 a–e The same as Fig. 7, except for the wind response at $\sigma=0.995$



anomalies slightly weaker than those in the CMIP5 results (Fig. 5a). The heat source (sink) in Fig. 8a is the combination of those in Fig. 8b–e. The vertical profiles are all set following the gamma distribution, which approximately matches the observed/CMIP5 profile. For the heat sink over the southeastern IO, though not consistent between models, its role is studied since it may partly contribute to the MME response.

The anticyclonic response in the upper troposphere mainly results from the condensational heating over the Bay of Bengal and the equatorial western Pacific. Figure 7 shows the wind response at $\sigma=0.12$ to heat source (sink). In the simulation where the LBM is forced by the combination of the four heat sources (sink), the upper troposphere shows a distinct anticyclone over South Asia and East Asia (Fig. 8a). Over South Asia, the anticyclone locates in the south of the climatological SAH, favoring the southward movement of the SAH, while the anticyclone excessively extends northeastward relative to that in the CMIP5 MME. It is clear that the anticyclone is mainly due to the heat source in the Bay of Bengal, except that the anticyclone is slightly poleward (Fig. 8b). In either experiment where the LBM is forced by heat source in the northern tropical IO or the southeastern equatorial IO, the circulation response is weak (Figs. 7d and 8c). It may due to the weak intensities and small regions of the two heat sources. In Fig. 8e, as the atmosphere is forced by the

heat source over the equatorial western Pacific, the whole tropic is warmed (Chiang and Sobel 2002). It strengthens the thermal contrast between tropics and extra-tropics, resulting in the anomalous westerly in the upper troposphere over subtropical Asia. Assuming that the westerly is imposed on the anticyclone in Fig. 8b, the zero line of zonal wind moves southward, as well as the anticyclone. It is evident by comparing a with b of Fig. 8.

In turn, the condensational heating favors the surface wind response in the CMIP5 MME. Figure 9 shows the wind response at $\sigma=0.995$ to heat source (sink). When the LBM is forced by the combination of the four heat sources (sink), the anomalous easterly over the equatorial IO, the anomalous

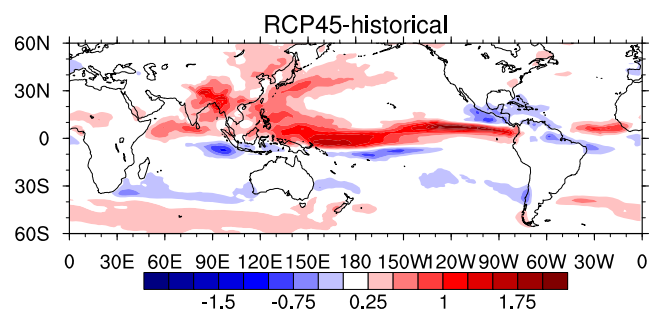


Fig. 10 The precipitation (color shaded, unit: millimeters per day) differences between RCP45 and historical simulation

westerly over the equatorial western Pacific, and the intensified southwesterly monsoon flow over the Arabian Sea can be reasonably forced (Fig. 9a). It implies that responses of the forementioned precipitation and the changes in the surface wind are coupled. For the equatorial IO easterly anomaly, the heat source over the Bay of Bengal, the northern tropical IO, and heat sinks over the southeastern equatorial IO are responsible (Fig. 9b–d). For the anomalous westerly over the equatorial western Pacific, only the local heat source may account for it (Fig. 9e). For the enhanced South Asia monsoon southwesterly, the condensational heating over the Bay of Bengal and the southeast equatorial IO make the positive contribution (Fig. 9b, d), while those over the northern tropical IO and the equatorial western Pacific may cancel the enhancement (Fig. 9c, e).

7 Summary and discussion

Based on NCEP-NCAR reanalysis, CMAP, HadISST, 17 CMIP5 model results, and the LBM simulations, this study investigates the SAH and the underlying precipitation responses to anthropogenic forcing and the possible link between them as well. The CMIP5 historical simulation reasonably reproduces the upper troposphere circulation (including the SAH), the underlying precipitation, circulation, and moisture.

Under global warming, the SAH moves southeastward and more than 75 % of the CMIP5 models project the equatorward shift. In individual models, the models showing stronger anticyclonic circulation in S SAH than that in N SAH tend to project more significant southward shift and vice versa.

The precipitation response displays a dipole feature: decrease over the southeastern equatorial IO and increase over the tropical northern IO, the Bay of Bengal, and the equatorial western Pacific. The increases are able to be consistently projected by the models, while the decrease is not. Among the regional rainfall changes, those over the Bay of Bengal and the equatorial western Pacific mainly account for the equatorward shift of the SAH. Over the Bay of Bengal, the rainfall-induced latent heat forces anomalous anticyclone at 100 hPa over the south of the SAH's climatological position; the rainfall response over the equatorial western Pacific leads to tropospheric warming in global tropics, contributes to the westerly over subtropical Asia, and shifts the Bay of Bengal rainfall-forced anticyclone further southward. For the rainfall over the northern tropical IO and the southeast equatorial IO, their influences on upper troposphere circulation are rather weak maybe due to the weakness and small areas of the heating.

The precipitation and the surface wind responses over the Indo-Pacific region are well coupled. On one hand, the surface wind anomaly affects the rainfall response. The easterly

change over the equatorial IO associated with the weakened Walker circulation causes evaporation and thermocline change, leading to the enhanced (subdued) warming over the tropical northern IO (the southeastern equatorial IO). For the northern tropical IO, though the increased SST favors the upward motion-induced rainfall, the moisture contributes more to the rainfall increase. For the Bay of Bengal, it is the enhancement of the South Asia monsoon southwesterly that transports more moisture there, resulting in the increased rainfall locally. Over the equatorial western Pacific, the weakened surface wind partly contributes to the underlying SST increase, favors the enhanced upward motion, and intensifies precipitation under RCP45.

On the other hand, the regional rainfall changes sustain the surface wind response. It is found that (1) for the equatorial IO easterly anomaly, the heat source over the Bay of Bengal, the northern tropical IO, and heat sinks over the southeastern equatorial IO are responsible; (2) for the anomalous westerly over the equatorial western Pacific, only the local heat source may account for it; and (3) for the enhanced South Asia monsoon southwesterly, the condensational heating over the Bay of Bengal and the southeast equatorial IO make positive contribution.

In the LBM, it is not clear why the anticyclone in response to all the four heat sources (sink) excessively extends northeastward in the upper troposphere over East Asia (Fig. 8a). A hint may be provided by the results of the heat source on the equatorial western Pacific. The westerly over subtropical Asia led by the heating-induced tropospheric warming favors the shrink of the northeastward extension of the anticyclone response (Fig. 8a, b, e). In addition, under global warming, apparent rainfall response is also seen in the tropical eastern Pacific and the tropical Atlantic (Fig. 10). The associated latent heating may benefit the tropospheric warming in global tropics, as well as the upper troposphere westerly response in subtropical Asia. It may further limit the northeastward extension of the anticyclone response, resulting in a more similar anomalous anticyclone to that in the CMIP5 MME results.

Acknowledgments We acknowledge the World Climate Research Programme's Working Group on Coupled Modelling, which is responsible for CMIP, and we thank the climate modeling groups (listed in Table 1 of this paper) for producing and making available their model output. For CMIP, the U.S. Department of Energy's Program for Climate Model Diagnosis and Intercomparison provides coordinating support and led the development of software infrastructure in partnership with the Global Organization for Earth System Science Portals. Besides, we wish to thank Prof. Renguang Wu for the insightful comments that lead to a significant improvement to the manuscript. The study was supported by the National Basic Research Program of China (grant NO. 2012CB955604), Open Research Fund Program of Plateau Atmosphere and Environment Key Laboratory of Sichuan Province Grants PAEKL-2013-K2 and PAEKL-2014-K2, and the National Natural Sciences Foundation of China (grant nos. 41205050 and 91337105).

References

- Boos WR, Kuang Z (2010) Dominant control of the South Asian monsoon by orographic insulation versus plateau heating. *Nature* 463(7278):218–222
- Chiang JCH, Sobel AH (2002) Tropical tropospheric temperature variations caused by ENSO and their influence on the remote tropical climate. *J Clim* 15:2616–2631
- Dethof A, O'Neill A, Slingo JM, Smit HGJ (1999) A mechanism for moistening the lower stratosphere involving the Asian summer monsoon. *Q J R Meteorol Soc* 125(556):1079–1106
- Duan AM, Wu GX (2005) Role of the Tibetan Plateau thermal forcing in the summer climate patterns over subtropical Asia. *Clim Dyn* 24(7–8):793–807
- Duan A, Hu J, Xiao Z (2013) The Tibetan Plateau summer monsoon in the CMIP5 simulations. *J Climate* 26:7747–7766. doi: <http://dx.doi.org/10.1175/JCLI-D-1112-00685.00681>
- Flohn H (1960) Recent investigations on the mechanism of the “Summer Monsoon” of Southern and Eastern Asia. Symposium on monsoons of the world, New Delhi. Hind Union Press, In, pp 75–88
- Held IM, Soden BJ (2006) Robust responses of the hydrological cycle to global warming. *J Climate* 19(21):5686–5699
- Hoskins BJ, Rodwell MJ (1995) A model of the Asian summer monsoon. Part I: the global scale. *J Atmos Sci* 52(9):1329–1340
- Hsu P, Li T (2012) Is “rich-get-richer” valid for Indian Ocean and Atlantic ITCZ? *Geophys Res Lett* 39(13), L13705
- Huang R, Sun F (1992) Impact of the tropical western Pacific on the East Asian summer monsoon. *J Meteorol Soc Jpn* 70(1):243–256
- Huang R, Wu Y (1989) The influence of ENSO on the summer climate change in China and its mechanism. *Adv Atmos Sci* 6:21–32
- Huang R, Huang G, Ren B (1999) Advances and problems needed for further investigation in the studies of the East Asian summer monsoon. *Chin J Atmos Sci* 23(2):129–141
- Jiang XW, Li YQ, Yang S, Wu R (2011) Interannual and interdecadal variations of the South Asian and western Pacific subtropical highs and their relationship with the Asian-Pacific summer climate. *Meteorol Atmos Phys* 113:171–180
- Kalnay E, Kanamitsu M, Kistler R, Collins W, Deaven D, Gandin L, Iredell M, Saha S, White G, Woollen J (1996) The NCEP/NCAR 40-year reanalysis project. *Bull Amer Meteor Soc* 77(3):437–471
- Li Q, Jiang JH, Wu DL, Read WG, Livesey NJ, Waters JW, Zhang Y, Wang B, Filipiak MJ, Davis CP (2005) Convective outflow of South Asian pollution: a global CTM simulation compared with EOS MLS observations. *Geophys Res Lett* 32:L14826. doi: [10.1029/2005GL022762](https://doi.org/10.1029/2005GL022762)
- Liu Y, Wu G, Liu H, Liu P (2001) Condensation heating of the Asian summer monsoon and the subtropical anticyclone in the Eastern Hemisphere. *Clim Dyn* 17(4):327–338
- Mason RB, Anderson CE (1963) The development and decay of the 100-MB summertime anticyclone over Southern Asia. *Mon Weather Rev* 91(1):3–12
- Meehl GA, Goddard L, Murphy J, Stouffer RJ, Boer G, Danabasoglu G, Dixon K, Giorgetta MA, Greene AM, Hawkins E (2009) Decadal prediction. *Bull Am Meteorol Soc* 90(10):1467–1485
- Park M, Randel WJ, Kinnison DE, Garcia RR, Choi W (2004) Seasonal variation of methane, water vapor, and nitrogen oxides near the tropopause: satellite observations and model simulations. *J Geophys Res* 109:D03302. doi: [10.1029/2003JD003706](https://doi.org/10.1029/2003JD003706)
- Randel WJ, Park M (2006) Deep convective influence on the Asian summer monsoon anticyclone and associated tracer variability observed with Atmospheric Infrared Sounder (AIRS). *J Geophys Res* 111(D12):D12314. doi: [10.1029/2005JD006490](https://doi.org/10.1029/2005JD006490)
- Rayner NA, Brohan P, Parker DE, Folland CK, Kennedy JJ, Vanicek M, Ansell TJ, Tett SFB (2006) Improved analyses of changes and uncertainties in sea surface temperature measured in situ since the mid-nineteenth century: the HadSST2 dataset. *J Clim* 19(3):446–469
- Sampe T, Xie SP (2010) Large-scale dynamics of the Meiyu-Baiu rainband: environmental forcing by the westerly jet. *J Clim* 23(1): 113–134
- Tao SY, Chen LX (1987) A review of recent research on the East Asian summer monsoon in China. In: Chang CP, Krishnamurti TN (eds) *Monsoon meteorology*. Oxford University press, USA, pp 60–92
- Tao S, Zhu F (1964) The variation of 100mb circulation over South Asia in summer and its association with march and withdraw of West Pacific Subtropical High. *Acta Meteorol Sin* 34(4):385–395
- Thomson AM, Calvin KV, Smith SJ, Kyle GP, Volke A, Patel P, Delgado-Arias S, Bond-Lamberty B, Wise MA, Clarke LE (2011) RCP4. 5: a pathway for stabilization of radiative forcing by 2100. *Clim chang* 109(1):77–94
- Ueda H, Iwai A, Kuwako K, Hori ME (2006) Impact of anthropogenic forcing on the Asian summer monsoon as simulated by eight GCMs. *Geophys Res Lett* 33(6), L06703
- Watanabe M, Kimoto M (2000) Atmosphere-ocean thermal coupling in the North Atlantic: a positive feedback. *Q J R Meteorol Soc* 126(570):3343–3369
- Wu R, Chen L (1998) Decadal variation of summer rainfall in the Yangtze–Huaihe River valley and its relationship to atmospheric circulation anomalies over East Asia and western North Pacific. *Adv Atmos Sci* 15:510–522
- Xie P, Arkin PA (1997) Global precipitation: a 17-year monthly analysis based on gauge observations, satellite estimates, and numerical model outputs. *Bull Am Meteorol Soc* 78(11):2539–2558
- Zhang P, Yang S, Kousky VE (2005) South Asian High and Asian-Pacific-American climate teleconnection. *Adv Atmos Sci* 22(6): 915–923
- Zhao P, Zhu Y, Zhang R (2007) An Asian-Pacific teleconnection in summer tropospheric temperature and associated Asian climate variability. *Clim Dyn* 29(2):293–303
- Zhao P, Zhang X, Li Y, Chen J (2009) Remotely modulated tropical-North Pacific ocean–atmosphere interactions by the South Asian high. *Atmos Res* 94(1):45–60